DETERMINING THE MINERALOGY OF THE POLYHYDRATED SULFATE CLASS IN CAPRI CHASMA USING RADIATIVE TRANSFER MODELLING. K.M. Robertson and S.Wiseman. Dept. of Earth, Environmental and Planetary Sciences, Brown University, Providence, RI, 02912. kevin_robertson@brown.edu

Introduction: Extensive sulfate-bearing deposits have been identified throughout Valles Marineris [1]. These detections display strong H_2O and OH^- absorption features but can also lack distinctive cation absorptions [2] in which case they are classified as polyhydrated sulfates (PHS). PHS can either represent complex mixtures of multiple hydrated species' or a single higher-hydrate phase where the diagnostic weak absorptions are masked or muted. The mineralogical unknowns associated with the PHS class can result in loosely constrained interpretations of the hydrological history in certain regions of Valles Marineris.

In this study, we use a DISORT atmospheric correction [3-4] model coupled with Hapke Radiative Transfer Modeling [5-6] of CRISM data in the Capri Chasma region to 1) model subtle variations in OH^- and H_2O absorptions and 2) constrain the mineralogy of the monohydrated and polyhydrated sulfate classes.

Methods: Empirical volcano scan corrections and ratioed spectra can leave artifacts in the hydration bands and can pose significant challenges in comparing spectra from different images. The Discrete Ordinate Radiative Transfer (DISORT) model [7-8] atmospherically corrects CRISM spectra to units of Lambert albedo and helps to overcome these challenges.

Hapke's radiative transfer model is commonly used for spectral un-mixing for airless planetary surfaces [7-8]. Recently, binary clay-igneous mixtures [9] and binary clay-sulfate mixtures [10] were analyzed using Hapke's RTM with some success. The parameterization of the Hapke model used in this study is the same as that of Li and Milliken (2015) [8]. The model inputs are, the CRISM reflectance data after DISORT correction, viewing geometry (*i*, *e*, *g*) from CRISM DDR data, and end-member single scattering albedo and their densities.

The end-member reflectance spectra used in the un-mixing were measured in RELAB at Brown University under ambient conditions with an ASD fieldspec3 spectrometer configured with a viewing geometry of: i = 30°, e = 0°, g = 30°. A total of 45 end-members were simultaneously used in the modeling, which included silicates, phyllosilicates, sulfates, zeolites, and glass.

Preliminary modeling was performed on image FRT0000D3A4 in Capri Chasma. This image was chosen because the monohydrated sulfates (MHS) and PHS units are located in close proximity to one another and there is an absence of atmospheric ice (which can be difficult to model with the DISORT method). This region has also been studied by Flauhaut et al., (2010) providing a good comparison with our results [12].

The DISORT corrected CRISM reflectance spectra were converted to single scattering albedo which was then weighted using linear combinations of endmember single scattering albedos. The combination of minerals that provided the best RMS error in the least squares minimization routine were used with no concern for the overall abundances. A horizontal end-member was included in the model to account for unconstrained dust effects and unknown particle sizes, which was then normalized out of the final results. This method limits the effectiveness in obtaining quantitative information, however; it is shown to be effective as a qualitative mapping tool [11].

Results: A comparison of a DISORT retrieved Lambert Albedo and volcano scan corrected I/F spectrum from FRT0000D3A4 is shown in Fig.1. The Lambert albedo spectrum has a different overall spectral slope because dust aerosols have been corrected and the water-related mineral absorption near 1.9µm is better defined due to robust modeling of CO_2 atmospheric absorptions that overlap with this feature. These improvements yield more representative spectra which ultimately improves the quality of the modeling.

Major phases identified in the preliminary modeling (45 end-members) included, olivine, pyroxene, hexahydrite, kieserite, ferricopiapite, melanterite, kornelite, gypsum, and hydrated silica, which were then used for all subsequent modeling.

The kieserite (yellow) and hexahydrite (Blue) phases identified from the modeling were mapped (Fig. 2a) and compared to the corresponding spectral parameter map (Fig. 2b). The similarity between the two maps suggests that the model is able to easily pick out the kieserite bearing (MHS) phase and can reasonably reconstruct the spectral parameter map based on the presence of the 2.4 µm band and the shifting of the ~1.9 µm hydration band to longer wavelength (2.1 µm). Mapping of the PHS is more difficult due to the absence of the diagnostic features, and the model becomes more reliant on subtle differences in the spectral shapes.

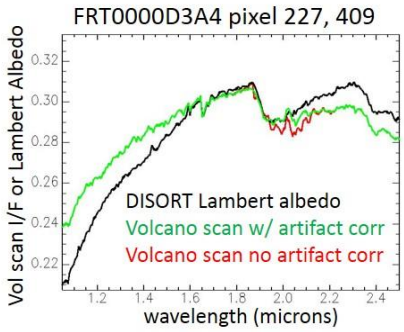

Figure 1. Comparison of DISORT retrieved Lambert Albedo and volcano scan corrected I/F spectrum from FRT0000D3A4.

Four distinct regions (A,B,C,D) were chosen (Fig.2) based on the preliminary modeling results, where C=PHS, D=MHS, and A and B=MHS + PHS. Representative spectra from the four distinct regions are shown in Fig. 3 with the corresponding modeled spectra overlain. The fits are all quite good with an average RMS error ~10^{-5} for all regions.

Comparing the spectral shapes (Fig.3) with the detected sulfate phases (Fig.4), it becomes apparent that the important spectral parameters are the slopes around the 1.5 µm region, the depth of the 2.4 µm feature and the depth, shape and position of the 1.9 µm feature.

In region A, we see a distinctly different concave shape to the 1.5 µm region and a sharp downturn at 1.2 µm, which is consistent with melanterite and ferricopiapite phases. The 1.9 µm region is very broad therefore the model must incorporate multiple hydrated end-members to match the overall shape which is consistent with the detection of kieserite and various polyhydrated sulfate phases.

In region C, the weak 1.9 um feature is shifted to shorter wavelengths which is consistent with the lower abundance of kieserite in the modeling results. Region D, however has the 1.9 µm feature shifted to longer wavelengths and is strongly correlated to high kieserite abundances and overall lower PHS abundances.

The detected sulfate phases are shown in Fig. 4 with some notable results being that a) Kieserite is highly variable b) hexahydrite is chosen over epsomite and c) there is an abundance of iron sulfate phases.

Conclusions: Due to the absence of diagnostic features in the spectra, the Hapke model is dependent on the subtle variations in the spectral shape; therefore the DISORT correction method is extremely important for proper phase identification.

Modeling results presented here have been shown to be effective at distinguishing between the MHS and PHS units. The model is adept at picking out the large kieserite units along with the more subtle kieserite layers. In addition, it is apparent that the model can also distinguish between subtle variations in the spectral shapes which is necessary for tracking mineralogical variability in the PHS units.

Not surprisingly, these results suggest that the different spectral classes are not limited to one mineralogical phase and likely represent complex mixtures. There are essentially three distinct units: a) kieserite rich (MHS) unit with low abundance of other sulfates b) a kieserite poor (PHS) unit which has high amounts of sulfate, particularly hexahydrite and c) a mixture of kieserite and sulfates.

The sulfate phases detected here are consistent with an iron/mg rich fluid which is not unexpected in these regions. The detection of hexahydrite over epsomite is an interesting observation with implications pertaining to the post-depositional paleoclimate.

Further work will focus on the two overlapping images (FRT000B385 and FRT000C564) in this region to test the consistency of the DISORT and Hapke models in terms of spectral shape and mineral detections. The rest of Capri Chasma will also be studied to understand the regional mineralogy.

References: [1]Gendrin et al., (2005) *Science, 307* [2]Cloutis et al., (2006) *Icarus, 184* [3]Stamnes et al., (1988) *Appl. Opt., 27* [4] Wolff et al. (2009), *JGR,114* [5] Hapke, (1981) *J. Geophys. Res, 86* [6]Hapke, (2005) *Cambridge University Press* [7]Poulet, (2004) *JGR., 109* [8] Li et al., (2015) *Met. and Pl. Sci., 50* [9] Ehlmann et al., (2011) *LPSC abstract #1704* [10] Robertson et al., (2013) *LPSC abstract #1614* [11] Robertson et al., (2015) *LPSC abstract #1462* [12] Flauhaut et al., (2010), *JGR, 115.*

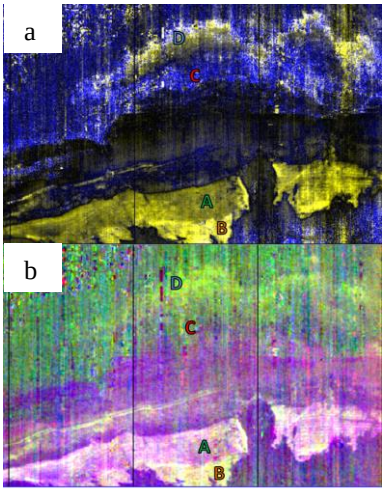

Figure 2. a) The modal abundance map for a subset of image FRT000D3A4 in Capri Chasma is shown here. (yellow = kieserite, blue = hexahydrite) **b)** spectral parameter map for the same image subset (R=SINDEX, R=BD2100, B=BD1900). with the pink and yellow areas representative of PHS and MHS units respectively. Four distinct regions are identified as A, B, C and D on both maps. These regions represent distinctly different areas as shown from the spectral parameters and the modeling.

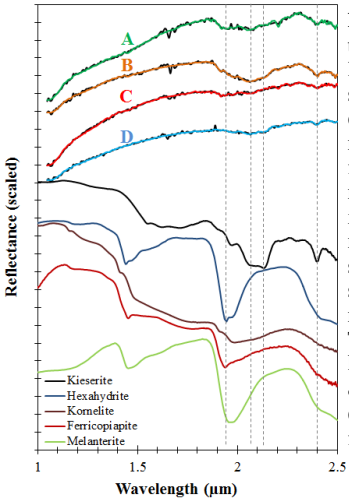

Figure 3. Crism spectra from the same subset of image FRT000D3A4. The modeled spectra are overlain and color coded to match the respective region that they were taken from (A, B, C, D). The modeled spectra fit quite well, ignoring CRISM artifacts and noise, while focusing on the spectral shape. The key sulfate phases identified in the modeling are also included. The stippled lines indicate the key absorption features that are determining the respective endmember contributions from the Hapke modeling.

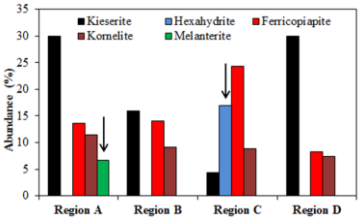

Figure 4. The modal abundances for the sulfate phases from the 4 regions in this study are shown here. Ferricopiapite and kieserite abundances vary widely while kornelite is fairly consistent. Arrows show the lone melanterite and hexahydrite phases.